Evaluation of Fugitive Dust Deposition Rates Using Lidar

Dennis Fitz and David Pankratz
College of Engineering-Center for Environmental Research and Technology
University of California, Riverside
1084 Columbia Avenue, Riverside CA 92507
dfitz@cert.ucr.edu

Russell Philbrick and Guangkun Li
Department of Electrical Engineering
The Pennsylvania State University
University Park, PA 16802
crp3@psu.edu

Proceedings of the U.S. Environmental Protection Agency's
11th Annual Emission Inventory Conference:
Emission Inventories-Applying New Technologies
San Diego, California April 29 – May 1, 2003

17 pages
2003

Evaluation of Fugitive Dust Deposition Rates Using Lidar

Dennis Fitz and David Pankratz
College of Engineering-Center for Environmental Research and Technology
University of California, Riverside
1084 Columbia Avenue, Riverside CA 92507
dfitz@cert.ucr.edu

Russell Philbrick and Guangkun Li
Department of Electrical Engineering
The Pennsylvania State University
University Park, PA 16802
crp3@psu.edu

ABSTRACT

Ambient measurements suggest that source inventories of PM_{10} from geologic sources are overestimated by 50 percent or more. This discrepancy may be due to inaccurate emission calculations and/or due to the rapid deposition of PM_{10} after entrainment into the atmosphere. A two-wavelength scanning backscatter lidar was used to investigate PM_{10} deposition rates from artificially generated fugitive dust. Dust was generated by vehicles on unpaved roads, a tilling operation, and from a blower fan, that dispersed known amounts of finely ground calcium carbonate or native soils. The size and concentration of the resulting dust plumes were monitored for up to a half-hour and a distance of several kilometers. The changes in these dust plumes' characteristics with time are depicted using a lidar to measure the relationship between backscatter and extinction at two wavelengths. An outdoor test chamber was prepared and used to examine the particulate size distribution and optical scattering properties of several different natural dust types and different preparations of powdered $CaCO_3$ samples under controlled conditions. These same materials were used to generate plumes for open atmosphere tests. Backscatter and extinction values calculated from models, based upon Mie theory for spherical particles, are compared to actual signals. These models show the dependence of optical backscatter and extinction upon the size, number density and refractive index of the particles. Thus, simultaneous measurements of the backscatter and extinction at two different wavelengths permitted the examination of settling rates of dust particles as a function of size. The larger particles, which contain most of the PM mass, settle out of the air fairly quickly, however, the fine particles contribute primarily to the backscatter, and remain suspended much longer. The results suggest that rapid deposition of PM_{10} particles, and the relatively longer residence time of the optical plume associated with small particles ($< 2\mu m$), may have led to overestimates of airborne particle mass in plumes.

INTRODUCTION

Geologic material is a major component of the airborne particulate matter in the western United States. Airborne particulate matter is an air quality concern because:

- Recent studies have associated increases in airborne particulate matter with increased morbidity and mortality, particularly in elderly and respiratory impaired individuals[2, 3, 4].
- Reduced visibility due to airborne particulate matter has both degraded the aesthetic beauty of natural views and affects activities such as the scheduled operation of air traffic.
- The changes in suspended airborne particulate matter alter the optical properties

of the atmosphere and may impact the radiative energy balance of the Earth's environment.

Source inventories for PM_{10} and $PM_{2.5}$ based on AP-42 algorithms show that geologic dust should contribute approximately 50% of the $PM_{2.5}$ in the western United States. Ambient measurements show that material of geologic origin typically contribute approximately 10% to the mass concentration[5]. There are several potential reasons for this discrepancy, the primary ones being inaccurate algorithms and data to calculate emission inventories and uncertainties of the lifetime of PM in the atmosphere.

Our overall objective of the project was to characterize the fate (deposition and transport) of PM emissions originating from mechanical disturbance of the soil (see Watson and Chow[5]). The results from the measurements will be used to validate the accuracy of the algorithms used to determine emission inventories from such sources. The study focuses on PM from unpaved roads and agricultural tilling. The tests also include artificially generated dust clouds of material of known size distribution to provide a validation of the analysis of the optical scattering properties and the algorithms for deposition of airborne particulate matter. The results allow a more accurate assessment of such fugitive dust sources to the regional PM concentrations. These assessments should then aid the formulation of cost-effective PM control strategies.

A specific objective of this project was to understand and define the differences between the measured and modeled concentrations of airborne dust carried in plumes from various sources. The results from the two measurement campaigns accomplished under this program during December 2000 and December 2001 have been analyzed and continue to hold our interest for investigations of the dynamical processes occurring in the planetary boundary layer. The preliminary results from the experiments conducted in December 2000 were presented during the last year.[1, 6, 7]

The interpretations and conclusions gained from the analysis of the results are discussed and example results that support the interpretations and conclusions are presented. The basic finding is that by combining measurements of the backscatter and extinction from the lidar with simple models demonstrates that the mass, represented primarily by the larger particles, settles out of a dust plume rapidly and results in a rapid decrease in optical extinction. The small particle fraction provides most of the optical backscatter and thus a plume carrying a relatively small amount of mass is still observed in backscatter for an extended period of time. This factor can be misleading and leads to an incorrect conclusion that the particle mass remains suspended for longer and is transported further than is actually the case. The simultaneous measurements of backscatter and extinction provide the clue that the model calculations of settling times must be reconsidered. The particle settling velocities in standard texts indicate longer residence times than those found in these experiments, and the results raise questions about what factors may contribute to a faster settling rate for the larger particles. The effective Stokes velocity is changed by turbulent motions and increase the migration for particles in a range of aerodynamic sizes. Motion of heavy particles is dominated by gravitational effects and very light particles are controlled by diffusion. In the normal surface layer, turbulence cells are present from generation by wind shears and by turbulent convection from surface heating and these must be considered.

The work was done in a test area where the generation conditions were controlled and where backscatter lidar could be safely used in the scanning mode to characterize the distribution of particulate matter. Tests were conducted by generating PM emissions to simulate emissions from vehicular travel on dirt roads and soil tilling operations. A series of individual test runs was conducted with data collected from real-time measurement methods.

RESEARCH APPROACH

The study was conducted at the University of California, Riverside, Agricultural Field Station in Moreno Valley, CA. The 720 acre facility is relatively level, except for some raised (~10 feet) dirt roads that run between some of the fields. There were no significant sources of PM around the facility. The project team coordinated with the UCR field site staff regarding any planned field plowing to avoid that activity during periods that tests were performed. The prevailing daytime winds were expected to be from the west during December.

A background meteorological station measuring wind speed (WS), wind direction (WD), temperature (T) and dew point (DP) was also located at this site. The meteorological tower instruments provided measurements of wind velocity at 2, 5, and 10 meters, temperature measurements at 2 and 10 meters, and net radiation measurements at 1.5 meters. The signals from the meteorological sensors were scanned once per second by a Campbell CR10X data logger and processed into ten-second averages.

The SESI scanning micro-pulse lidar (MPL) was located 500 to 800 meters away from the plume generation region during the December 2001 measurement program. The lidar provided the backscatter signal profiles at two wavelengths (523 and 1047 nm) and has several features that make it the ideal instrument for mapping the dust clouds to be generated in this program. The instrument has a scanning platform, which can be used to provide a mapping of the airborne particulate matter. The instrument is eye-safe but maintains high sensitivity by using high average power, obtained from operating at a high pulse repetition frequency (prf), and expansion of the beam to produce lower energy flux per unit area. The MPL measures the backscatter signal profiles at 1047 nm in the near infrared (NIR) and 523 nm in the mid-visible spectrum. These wavelengths are most sensitive to scattering from particle sizes in the size range near 1 μm, and they are separated sufficiently to provide some sensitivity to changes in fine particle size distributions. The lidar results were obtained by simultaneously integrating the signal returns for 2 seconds in range bins that are 33 meters in length for each of the wavelengths.

During the open atmosphere testing, a high-resolution digital video camera (Sony Digital DCR-VX700) was mechanically coupled to the lidar to document the distribution of the dust generated and to verify the lidar pointing direction. Images were taken at each scanning position by the camera mounted on the top of the lidar to follow the path of the laser beam and provide a clear picture of the area being scanned. The scanning lidar with the camera was located upwind of the generation point. The scan covered the region about 10-20° on either side of the centerline between the location of the lidar and the generation point. An inclinometer was mounted on the lidar to measure the elevation angle.

Open atmosphere measurements were obtained during both measurement programs using a blower to generate plume puffs from soil and from calcium carbonate dust, and by using a vehicle (truck or tractor) to generate off-road dust as shown in Figure 1. The blower device for generating dust puffs used a 5 horsepower centrifugal blower. During the pilot study in December 2000, limited testing was carried out using calcium carbonate (~10 μm size) and a fogger (propylene glycol) of the type used to provide special effects for the film industry. The December 2001 tests used many different sizes of $CaCO_3$ dust and sifted soil types from several locations; including the local field, soil from California locations of Shafter, Westside and Kearney. During the 2001 campaign, an additional type of measurement was undertaken using a test volume where particle concentrations could be measured using a controlled 10-meter chamber, as shown in Figure 2. The 10-meter chamber was located about 630 meters from the lidar instrument and aligned so that the beam could pass through the chamber. A target board was located beyond the chamber at a range of 700 meters. The beam is about 25 cm in diameter and could pass though the chamber without any scattering from the chamber walls. PM_{10}

concentrations were continuously monitored (TSI model 8520 DustTrak™ with 10μm size selective inlets) at the front, middle and back end of the chamber with a two second resolution. An optical particle counter (Climet Model Spectro 0.3) was used to determine the particle size distribution in sixteen channels from 0.3 to 20μm at the middle of the chamber, near the location where the sample was blown into the chamber.

The Scanning Micro-Pulse Lidar (MPL) used for these investigations was leased from Science and Engineering Services Inc. (SESI) and operated by the Penn State University graduate students. The instrument provides a backscatter signal at 2 wavelengths and has several features that make it the ideal selection for mapping the dust clouds to be generated in this experiment. The instrument has a scanning platform which can be used to provide a mapping of the airborne particulate matter. The instrument is eye-safe but maintains high sensitivity from using a high average power, obtained because of high operating prf (several kHz), and by expanding the beam to produce lower energy flux per unit area. Two Nd:YLF lasers are used at their fundamental and frequency doubled wavelengths of 1047 and 523.5 nm with energy outputs of approximately 10 and 5 μJ, respectively. The beams are expanded and transmitted through a 20 cm diameter telescope, which is also used to receive the backscattered signal. An avalanche photo-diode detector is used in a pulse counting mode to measure the returned signal at each of the two wavelengths. The instrument has several operating modes, however we selected the highest range resolution (33 meter data bins) and used a two-second integration of the signals for each profile. The most useful results are obtained by averaging the returns backscattered from the clear atmospheric path before generating a dust plume on the path. The results obtained by forming a ratio of the measured dust profile to that of the clear path then provides a measure of the optical backscatter and extinction signals associated with the generated dust plume.

The procedure for measurements in the chamber was to close the ends of the chamber, turn on the three fans located inside and then inject the dust. After one minute, the ends of the chamber were opened, fans turned off, and the laser beam measurements commenced. The lower panel in Figure 3 shows a sequence of three tests using the chamber. The sequence of events, which included closing of the chamber, injection of the dust puff and subsequent opening of the chamber, is clearly shown. The upper panel in Figure 3 displays the raw signal from the lidar during these same tests. The chamber and target board data are taken from the 19th and 21st range bins of the lidar corresponding to ranges of about 630 and 700 meters, respectively.

RESULTS

Only a small sample of the results obtained can be included in this paper. We have chosen to use a set of chamber tests and open air tests performed on one test day during the primary testing program in December 2001 as an example of the type on measurements obtained. The measurement record for chamber tests on19 December 2001 is summarized in Table 1. Figure 3 shows the raw lidar returns from the chamber and the target board and the signals from the DustTrak for the 0.7μm $CaCO_3$ tests #10 (50 mg), #11 (200 mg) and #12 (800 mg) on 19 December 2001. The measurements in Figure 3 from the Lidar and DustTrak show the signals change as the amount of material in the sample increases, 50, 200 and 800 mg, however the 50 mg signal is so small that those results are not very useful.

The upper panel of Figure 3 shows the signal return from the closed end on the chamber near 05:44, 05:50 and 05:55. When the chamber is opened, the lidar return from the dust in the chamber and the target board are observed. Since the chamber is only 10 meters in length (corresponding to only 1/3 of one range bin), the extinction signal is relatively weak and the hard target return is the only practical way to observe any extinction signal. Examination of the signals of the target board return shows that the extinction corresponding to the dust path can be detected. For example, the upper panel of Figure 3 at about 05:51 (test #11) shows the extinction signal at the same time as the larger return from the backscatter signal. When the backscatter

signal is highest, the return from the target board is reduced, however the S/N is not sufficient to permit a quantitative measure of the extinction value from the target board returns. The lower panel of Figure 3 shows the three DustTrak measurements (front, middle and back of chamber) together with the lidar signal return, which has been normalized to "1" by using measurements of the clear atmospheric path before the test. The lidar signal in the chamber is high before opening due to the back scatter from a white card placed on the front of the chamber. The backscatter from the dust is observed in the lidar return when the path is open but the concentration within the chamber volume is not sufficient to observe any path extinction on the atmospheric path. A comparison of these three tests (#10 - #12) shows some difference in the settling rate of the dust that is probably due to the fans not being turned off exactly at the same time in this case. The increase in signals with increasing sample size is easily observed. During a measurement period when the Climet spectrum was obtained (1 minute), the DustTrak data (two second step) was averaged and compared with the integrated value of particles less than 10 μm reported by the Climet instrument, and the comparison was quite good. The range of these instruments includes most of the particles contributing to the optical properties, since heavier particles settle quickly. The instruments are capable of measuring particles less than 20 μm (Climet) and 10 μm (DustTrak) respectively, and so the concentrations of larger particles are not characterized.

The particle size spectrum from the Climet instrument of the 0.7 μm $CaCO_3$ sample is shown in Figure 4. A two component log-normal distribution has been fit to the measured spectrum. The particle size spectra of the various $CaCO_3$ crush samples measured on 19 December 2001 are shown in Figure 5 from the tests using the 200 mg samples. The variations between these curves are small on a log scale, however, the observed variation agrees with expected changes. It is apparent that the 0.7 μm sample is anomalously low compared with the other samples. The lower particle concentration observed in the 0.7 μm tests may be due to poor disbursal during injection, or may be lost because of the particles adhering to the plywood sides of the chamber. Examination of Figure 5 shows that the relative signals change as expected for the other size distributions measured. The Climet instrument measurements of the 0.7 μm sample, that are shown in Figure 5, are presented as mass density and number density in Figure 6. We use the particle spectrum shown in Figure 6 to calculate the expected optical signal expected for the lidar and examine the expected variations when the larger particle sizes are removed from the distribution, this analysis is described at the end of this report.

The results shown in Figure 7 provide the Climet particle spectra for the several types of soils measured during the chamber tests. Soil samples included local sifted field soil and soil samples from several California sites, including Shafter, Westside and Kearney locations. In addition, the results from 2 and 10 μm samples of $CaCO_3$ and a standard of Arizona Road Dust were measured, and the results are shown in Figure 7. It is obvious that the $CaCO_3$ samples contain a larger relative concentration of the smaller particles than do the soil samples. Also the Arizona Road Dust contains a larger fraction of small particles than any of the other soil samples.

The open field tests of these samples were conducted by generating sample puffs using the blower generator. In Figure 8, the time sequences of the lidar measured backscatter peak values and the integrated extinction through the cloud are shown for Test #44, which is a 600 g sample of 0.7 μm $CaCO_3$. This plot shows the ratio of the signals relative to the background atmospheric path prior to the test. The interesting thing to note is that the backscatter signal remains high for quite a long time after the extinction signal has returned to pretest levels. The fact that there is such a large difference in the residence time for particles in the size range between 1 and 10 μm is recognized from the expected settling velocity shown in Figure 9.[8]

Figure 10 shows a typical experiment depicting the generation of a dust cloud generated with the blower unit as observed by the digital video camera mounted on top of the lidar instrument. The dust generation equipment was located at ranges from 150 to 800 meters in various test scenarios. The lidar was used to either point at the center of the plume, as presented

in Figure 8, or was scanned automatically to make a horizontal slice through the test volume, and the elevation angle could be adjusted manually. Using the scanning lidar, the plumes were generally tracked out to 1.5 km along the path and on radials, which were set to sweep up to ±30º horizontally. The plumes probably could have been tracked much longer, at least along some radials (up to the lidar's maximum range of 20-30 km). Because it was more desirable to obtain data over shorter ranges, plume tracking generally stopped when the plume drifted to ranges greater than about 1.5 km.

A simple model calculation based upon the scattering theory for spherical particles by Gustov Mie has been used to simulate first order effects observed. Mie theory calculations provide the scattering angle dependence for spherical particles with various indices of refraction.[6, 7] While the dust scattering studied in these experiments cannot be described as associated with spherical particles, it still provides a useful comparison of the scattering properties. In particular, the Mie theory results should provide accurate results for the smaller particles, where shape is less important, and the relationship between the forward and backward scatter intensities (extinction and backscatter) should provide useful insight for this investigation. The theory also provides information on the variations in the absorption of the particles due to their complex index of refraction. The Mie scattering theory used for this investigation is a straightforward application of the scattering intensity in the two polarization planes that comes directly from electromagnetic theory, and all of the applications here use only the 0º and 180º scattering intensity. Figure 11 shows model calculations of visible and NIR backscatter and extinction for several mono-disbursed particle diameters and for a range of particle concentrations. The calculation simulates a 200-meter-thick uniform dust cloud and calculates values at 30-meter intervals (same as the bin size of the lidar result). The figure shows the differences in backscatter and extinction signals as the density and size of particles is changed. It is important to notice that the extinction only depends on the concentration and size of particles and weakly on the wavelength of absorption. However, the backscatter does depend strongly on the wavelength. The calculations shown in Figure 11 demonstrate that the backscatter intensity and the extinction depend on the particle size. The relatively larger backscatter for the NIR wavelength is expected based upon the fact that the longer wavelength allows the particles to remain longer in the Rayleigh scattering range, where the cross-section dependence ($r^6 \sim 2^6 = 64$) results in increased scattering. Increasing the particle size increases the backscatter up to the point where the scattering loss results in an optical thickness that reduces the backscatter signal. The value of using the results from the mono-disbursed distribution of particles depicted in Figure 11 is limited because real particle distributions always contain a significant range of particle sizes. However the same calculations can be carried out for a range of particles sizes, as shown in the following example.

The lidar backscatter signals and extinction from passing through the dust cloud that was generated by the blower unit are shown in Figure 12. These curves are obtained by comparing with the backscatter signal before the dust was generated, the signal strength starts increasing at the front edge of dust plume and forms a peak in the center of cloud. The backscatter coefficient can be estimated from the signal magnitude. After the laser beam passes through the cloud, there is a sudden drop of backscatter signal due to the attenuation of the laser beam. The extinction coefficient can be estimated by the attenuation amount, which is the signal drop after the laser signal passing through the dust plume. If we assume the dust particles inside the cloud are uniform and spherical, a certain relationship should exist between the values of backscatter and extinction coefficients that correspond to a dust plume with given set of particle sizes. This will allow us to simulate the laser backscatter profile passing through the cloud and specify the dust particle size and density from the analysis of the simulation.

Figure 12 shows one example from the 19 December 2001 test (#44) for the case of 0.7 μm calcium carbonate cloud containing 600 grams of material. Notice that the magnitude of the backscatter and extinction are similar to the values that would be expected from the simulation

shown in Figure 11(a). After release, the backscatter signal does not change very much during the next two minutes (4 profiles) while the extinction is observed to recover. This point is even better observed in the presentation of the same results in Figure 8. The small particles in the sample material are sufficiently small that the settling time is slow, however the rapid recovery of the extinction is observed as the larger dust particles settle out of the sample.

The model calculations, shown in Figure 13, depict the backscatter and extinction which would be expected for the sample of 0.7 μm $CaCO_3$ particles represented in Figure 6, which shows the particle size spectrum for this material. The calculations shown in Figure 13 represent the changes which are expected to occur as the particles larger than a certain size are removed. The particle distribution shown in Figure 6 is truncated for particles greater than selected sizes to calculate the optical properties. The calculation is intended to represent the changes that would be expected for the case of larger particles settling from the distribution. It is interesting to see that this simple calculation does have many similarities to the results shown in Figure 12. The magnitude of the backscatter and extinction calculated from the particle size spectrum does agree well with the measured lidar profiles. The changes in the backscatter and extinction calculated from truncating the particle spectrum agree quite well with the time sequence of measured profiles. These comparisons show that the relative changes in the backscatter and extinction profiles are representative of the settling of larger particles from the airborne sample.

The experimental backscatter and extinction measurements can now be examined in the context of the simulation calculations. Progress has been made on the more difficult task of using the field measurements to solve the inverse problem and describe the particulate matter properties from the scattering profiles. Our goal is to describe size and distribution of the airborne PM and to show the variation in the settling rate of the particulate matter from various sources. The analysis is aimed at developing the inversion algorithm for fully describing the changes in particle size within the generated dust clouds.

CONCLUSIONS

Optical scattering measurements using lidar have been examined for each of the several tests using native soils and sized calcium carbonate samples to generate dust plumes, and some examples of these results are presented here. A set of measurements has been obtained using a 10-meter chamber to simultaneously measure the optical scattering properties with a lidar and with measurements of the particle density and size distribution. The model calculations show that extinction is more dependent on larger particle sizes. Based on the analysis of results obtained, the settling rates of the larger particle component result in reduction in the optical extinction prior to the decrease in backscatter signals, which are dependant on the scattering from a larger number of smaller particles. The analysis and interpretation from the data collected on fugitive dust of various types will be carried out using the lidar data obtained. The preliminary conclusion is that the rapid settling rate of the larger particles results in the lower quantity of fugitive dust as a fraction of emission inventory. The backscatter signals from small particles, which have a longer residence time, result in a much longer apparent residence time of airborne fugitive dust, however, the observed plume may not carry a significant fraction of particle mass. The data will be used to critically examine the settling rates for the various particle sizes. Even though the aerodynamic settling velocity of the airborne particles through the atmosphere has been studied for many years, the additional effects from turbulence generated by surface wind shear and by convection may also change the residence times expected for various particle sizes.

REFERENCES

1. Fitz, D., D. Pankratz, R. Philbrick, and G. Li: "Evaluation of the Transport and Deposition of Fugitive Dust Using Lidar," Proc. Environmental Protection Agency's 11th Annual Emission Inventory Conference: Emission Inventories-Partnering for the Future, Atlanta GA (2002)
2. Magari, S.R., R. Hauser, J. Schwartz, P.L. Williams, T.J. Smith, and D.C. Christiani: "Association of Heart Rate Variability with Occupational and Environmental Exposure to Particulate Air Pollution," *Circulation* 104, 986-991, 2001.
3. Peters, A., D.W. Dockery, J.E. Muller, and M.A. Mittleman: "Increased Particulate Air Pollution and the Triggering of Myocardial Infarction," *Circulation* 103, 2810-2815, 2001.
4. Mauderly, J., L. Neas, and R. Schlesinger: "PM Monitoring Needs Related to Health Effects," *Proc. PM Measurements Workshop*, EPA Report No. 2, Chapel Hill, NC, pp 9-14, July 1998.
5. Watson, J.G., J.C. and Chow: "Reconciling Urban Fugitive Dust Emissions Inventory and Ambient Source Contribution Estimates: Summary of Current Knowledge and Needed Research," Document No. 61110.4D2, Desert Research Institute, Reno NV, September 3, 1999.
6. Li, G., S.N. Kizhakkemadam, and C.R. Philbrick: "Optical Scattering by Airborne Dust Particles," Proc. Air Force Optical Transmission Meeting, Hanscom AFB, MA, June 2001.
7. Li, Guangkun, Sachin J. Verghese, C. Russell Philbrick, Dennis Fitz and David Pankratz: "Airborne Dust and Aerosols Description Using Lidar Backscatter," 25th Annual Conference on Atmospheric Transmission and Radiance Models, Lexington, MA, June 2002.
8. Seinfeld, J.H and S.N, Pandis: *Atmospheric Chemistry and Physics: From Air Pollution to Climate Change*, Wiley-Interscience, 1998.

ACKNOWLEDGEMENTS

We wish to thank Patrick Gaffney and the California Air Resources Board for funding this research. We appreciate Tony Taliaferro's assistance in setting up the equipment used in this study. The efforts of Sriram Kizhakkemadam and Gregg O'Marr significantly contributed to the lidar results and were important for the successful data collection.

DISCLAIMER

The statements and conclusions in this report are those of the researchers and universities and not necessarily those of the California Air Resources Board. The mention of commercial products, their source, or their use in connection with material reported herein is not to be construed as actual or implied endorsement of such products.

Table 1. Tests, which were conducted 19 December 2003 using a test chamber (#1 - #37) and open atmosphere puffs (#38 - #55), were followed by several tests on dust generated by a plowing tractor.

Test	Material	Amount	Size
#1	$CaCO_3$	50 mg	0.7 µm
#2	$CaCO_3$	200 mg	0.7 µm
#3	$CaCO_3$	800 mg	0.7 µm
#4	$CaCO_3$	50 mg	2 µm
#5	$CaCO_3$	200 mg	2 µm
#6	$CaCO_3$	800 mg	2 µm
#7	$CaCO_3$	50 mg	4 µm
#8	$CaCO_3$	200 mg	4 µm
#9	$CaCO_3$	800 mg	4 µm
#10	$CaCO_3$	50 mg	10 µm
#11	$CaCO_3$	200 mg	10 µm
#12	$CaCO_3$	800 mg	10 µm
#13	$CaCO_3$	50 mg	15 µm
#14	$CaCO_3$	200 mg	15 µm
#15	$CaCO_3$	800 mg	15 µm
#16	Az Road dust	50 mg	
#17	Az Road dust	200 mg	
#18	Az Road dust	800 mg	
#19	UCR dust	50 mg	< 425 µm
#20	UCR dust	200 mg	< 425 µm
#21	UCR dust	800 mg	< 425 µm
#22	Kearney	50 mg	
#23	Kearney	200 mg	
#24	Kearney	800 mg	
#25	Kearney	3.2 g	
#26	Westside	50 mg	
#27	Westside	200 mg	
#28	Westside	800 mg	
#29	Westside	3.2 g	
#30	Shafter	200 mg	
#31	Shafter	800 mg	
#32	Shafter	3.2 g	
#33	$CaCO_3$	50 mg	0.7 µm
#34	$CaCO_3$	200 mg	0.7 µm
#35	$CaCO_3$	800 mg	0.7 µm
#36	$CaCO_3$	50 mg	2 µm
#37	$CaCO_3$	200 mg	2 µm
#38	$CaCO_3$	300 g	4 µm
#39	$CaCO_3$	300 g	75 µm
#40	Kearney	300 g	< 425 µm
#41	Kearney	1.5kg	< 425 µm
#42	$CaCO_3$	600 g	0.7 µm
#43	$CaCO_3$	600 g	10 µm
#44	$CaCO_3$	600 g	0.7 µm
#45	$CaCO_3$	600 g	4 µm
#46	$CaCO_3$ mix	600 g	300g@4µm 300g@15µm
#47	$CaCO_3$	600 g	15 µm
#48	Shafter	600 g	< 70 µm
#49	$CaCO_3$	600 g	15 µm
#50	$CaCO_3$	600 g	100 µm
#51	$CaCO_3$	600 g	200 µm
#52	$CaCO_3$	600 g	100 µm
#53	$CaCO_3$	600 g	4 µm
#54	Westside	900 g	< 425 µm
#55	Westside	900 g	< 425 µm

(a)

(b)

(c)

Figure 1. Open air generation of dust plumes: (a) blower used to generate plume of dust from sifted soil, (b) blower generated plume of $CaCO_3$, (c) dust plume from a tractor plowing.

Figure 2. Chamber was used to generate and measure a controlled sample (clockwise views): (a) Front (west) and north sides of test chamber where samples are injected and measurements made, the chamber is shown with instrumented meteorological tower, (b) DustTrak optical scatter instruments (10 µm size orifice) and Climet particle spectrometer (16 channels - 0.5 to 10 µm), (c) View of lidar from back of chamber at range of 450 meters thru the chamber (notice fans used to circulate the sample), (d) View of the east side of 10-meter chamber.

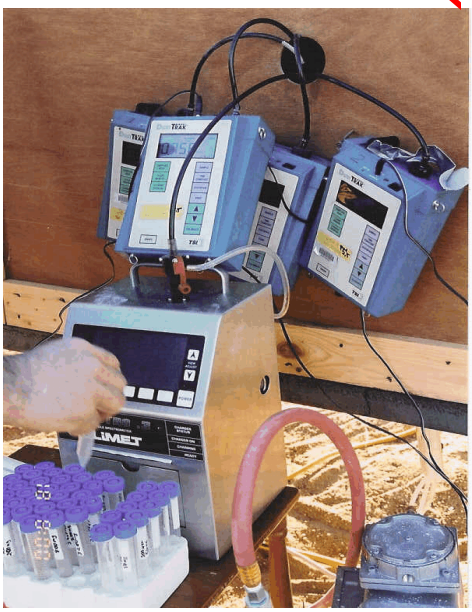

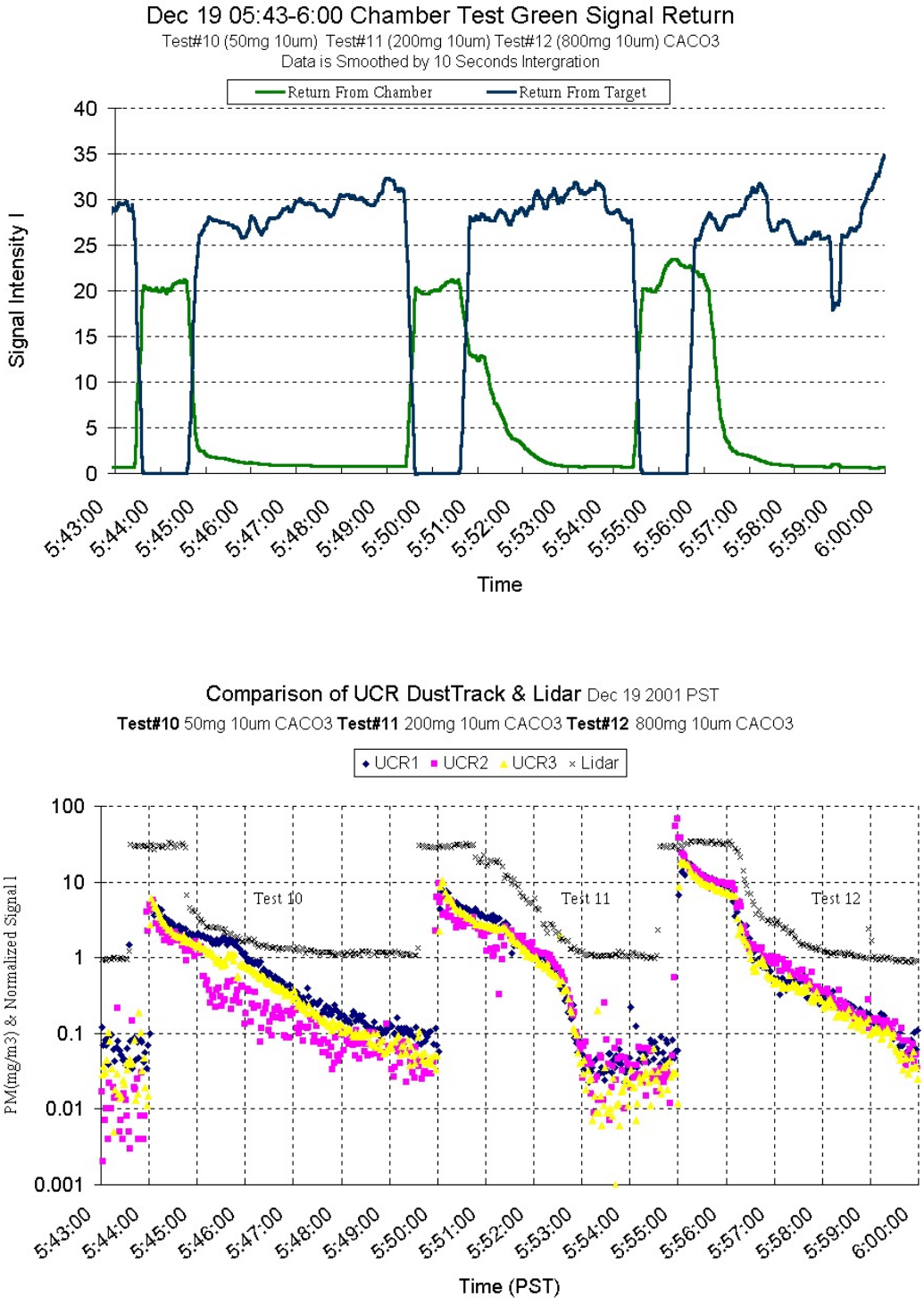

Figure 3. The chamber test measurements from Tests #10, #11 and #12 are shown. Upper panel shows the raw signal returns from the lidar at the range intervals corresponding to the chamber and the target board. The lower panel shows the signal from the DustTrak instruments and the normalized lidar return.

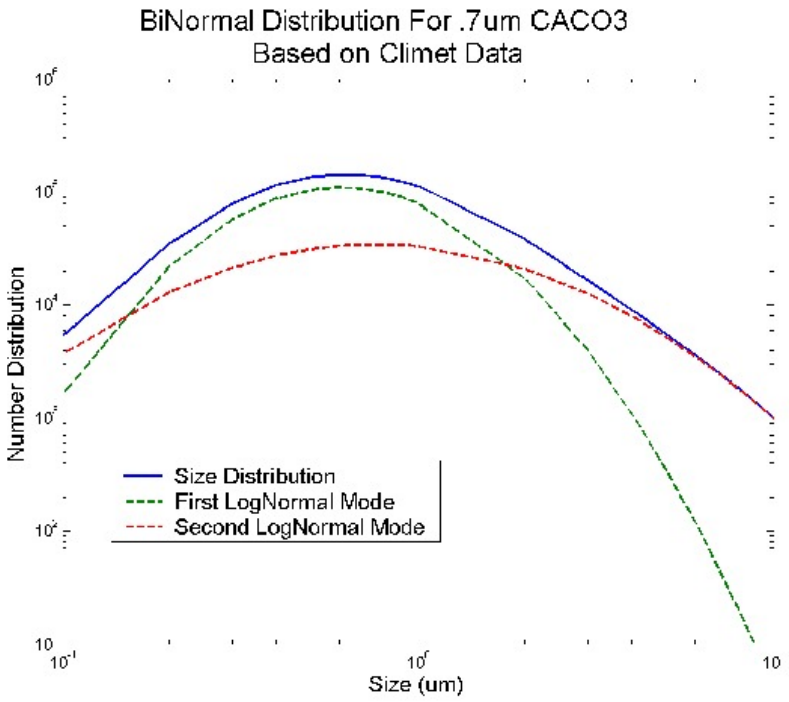

Figure 4. The log-normal distributions for a two components are fit to the Climet instrument measured curve for the 0.7 μm sample of $CaCO_3$.

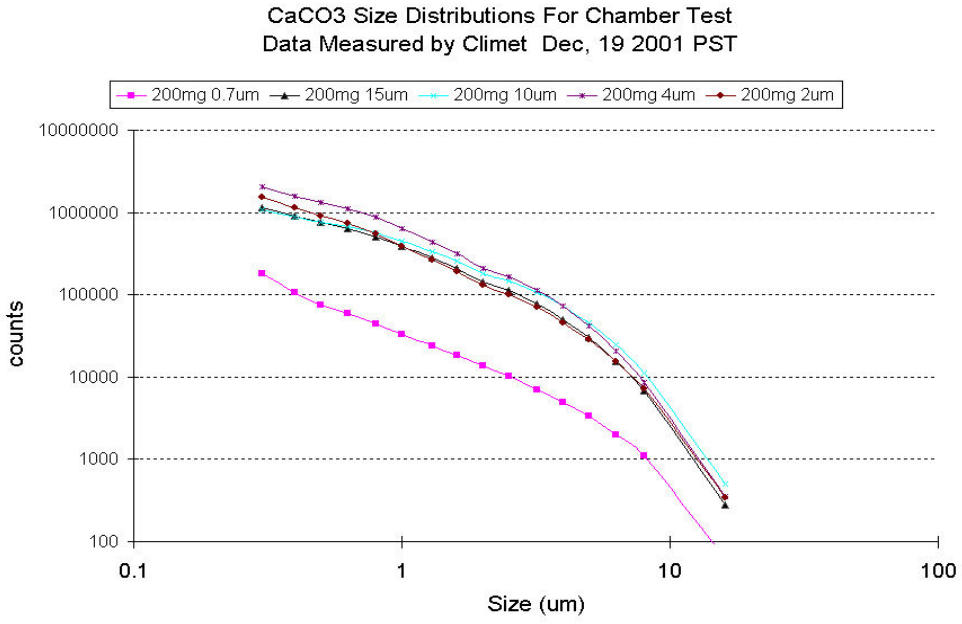

Figure 5. The Climet spectrum of the particle counts versus particle size for the several samples of $CaCO_3$ power that were used during the testing. Notice that the 0.7 μm case is an anomaly (see text) and the other samples do show a change that agrees with the increasing size of the samples.

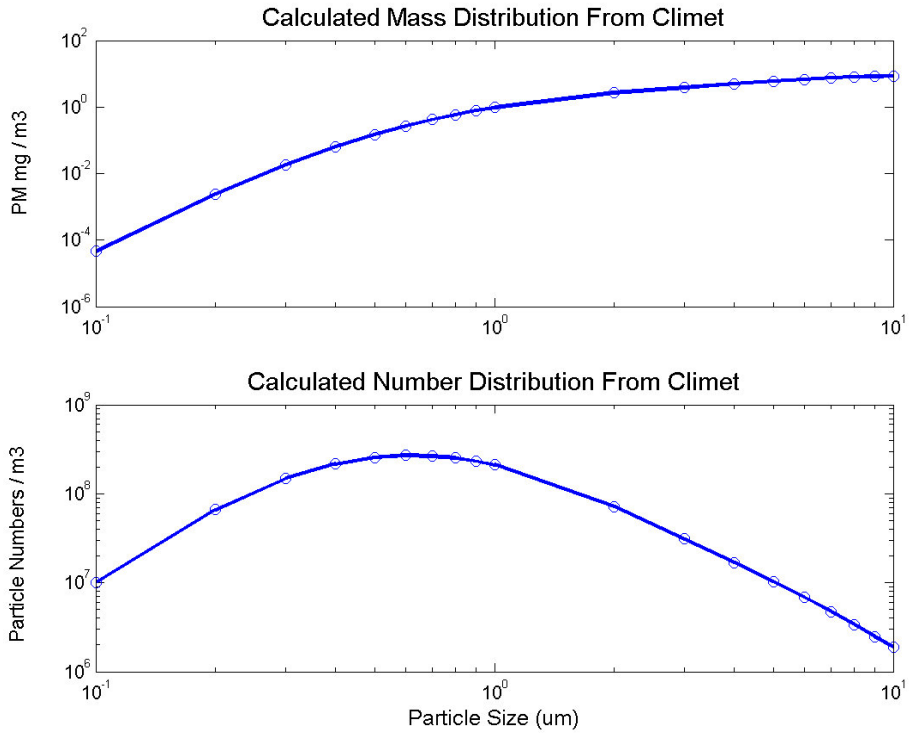

Figure 6. The Climet spectrum for the 0.7 μm sample of the $CaCO_3$ dust is shown for the measurements in Figure 5 converted to number density and to mass density.

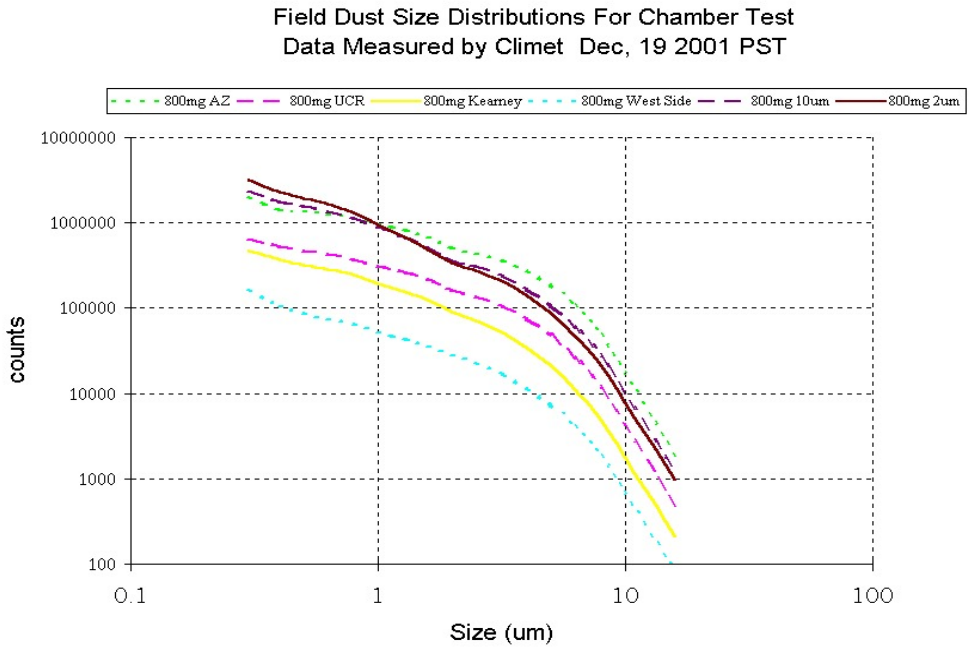

Figure 7. The Climet particle size spectra for the several different types of soil and powder used during the test are compared.

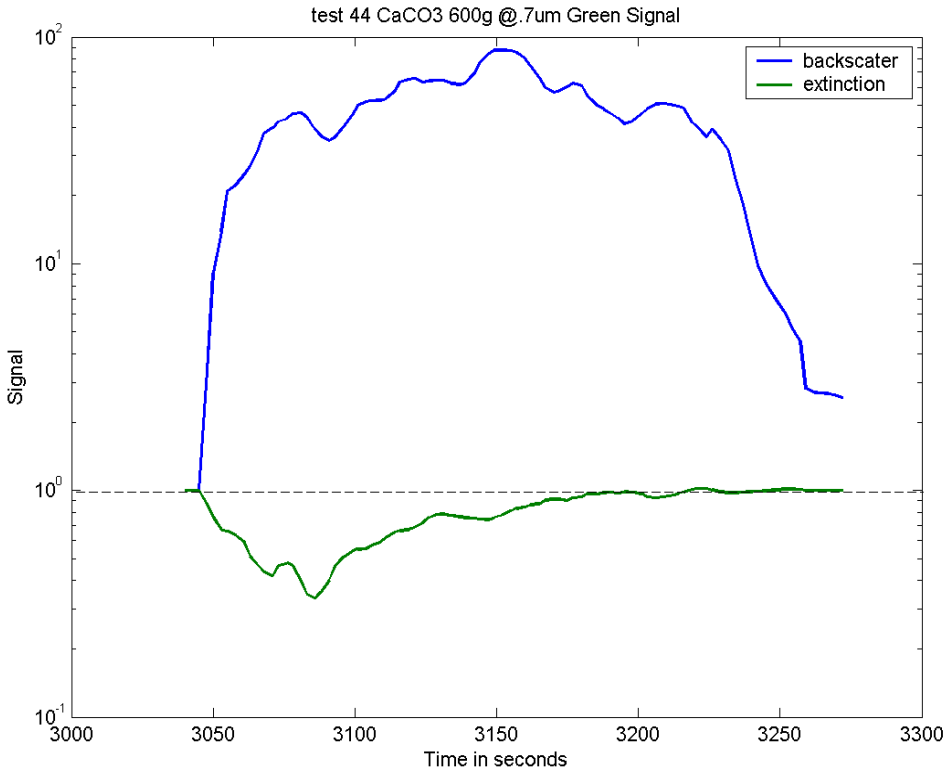

Figure 8. The open air time sequence of the lidar backscatter peak values and extinction values are shown for profiles of Test #44 on 19 December 2001 for the 0.7 μm $CaCO_3$ 600 g sample.

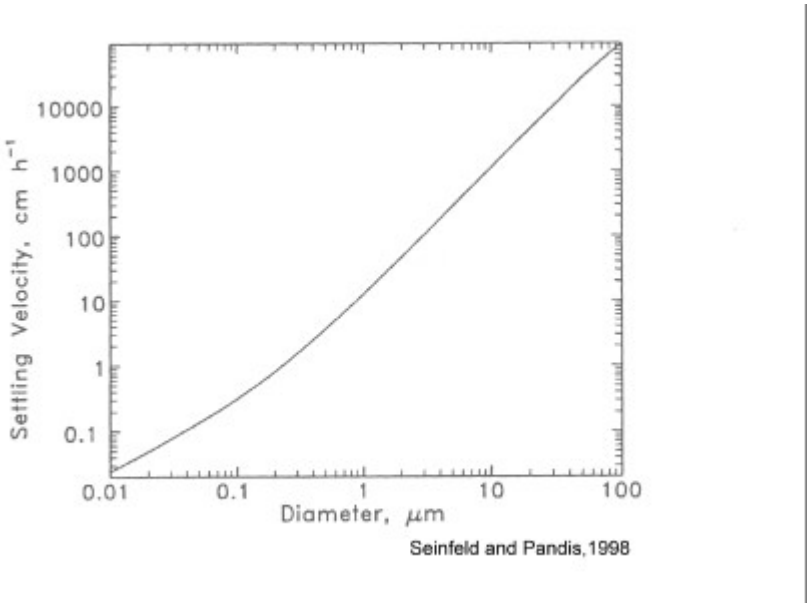

Figure 9. The expected settling velocity versus particle diameter from standard text (Seinfeld and Pandis[8]).

T+1 sec T+30 sec

T+60 sec T+90 sec

Figure 10. Example of a puff plume of local soil that is tracked by scanning lidar.

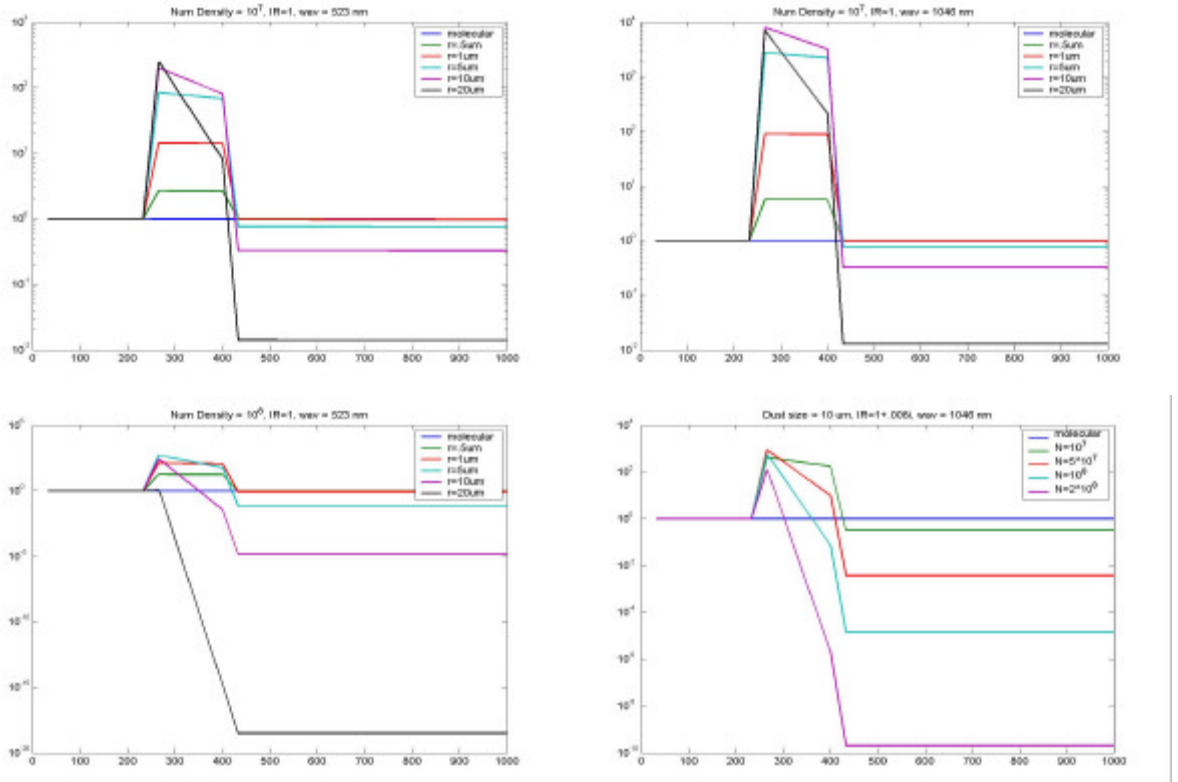

Figure 11. The calculations of the optical scattering properties expected for different size and density of particles are shown for the two wavelengths.

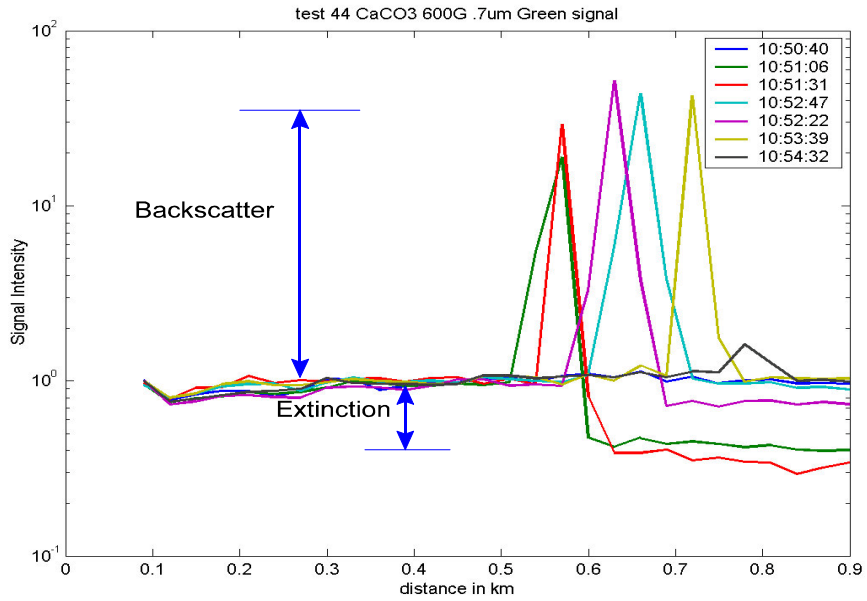

Figure 12. The results from Test #44 on 19 December 2001 show several of the lidar profiles that show the time variation in the backscatter and the extinction measured by the lidar. These range profiles are from the same data set that is shown in Figure 8.

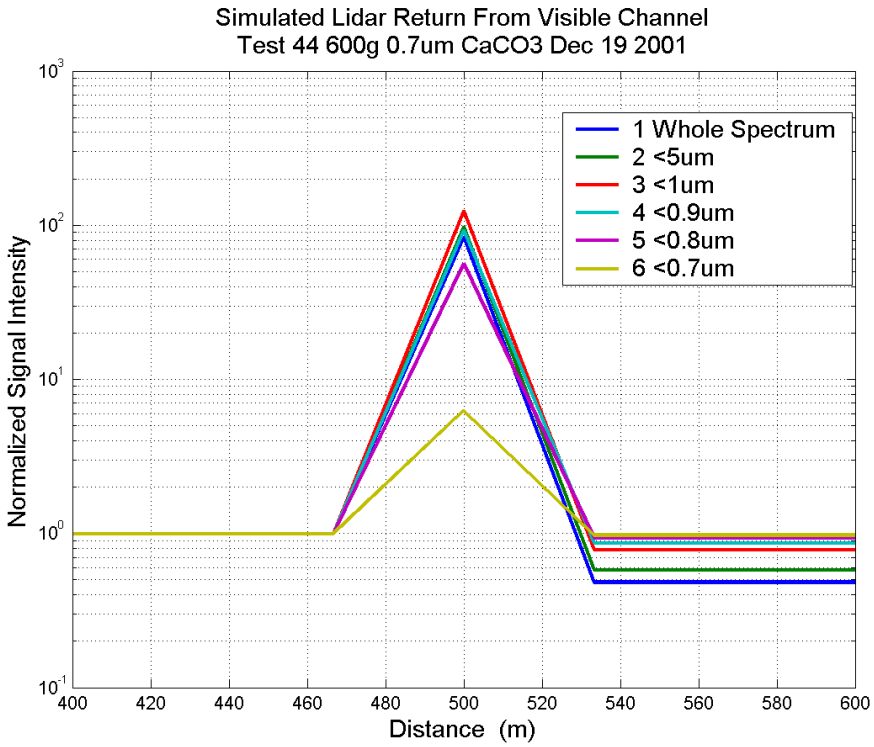

Figure 13. The results from a calculation of the backscatter and extinction expected when one sequentially removes the larger end of the spectrum of the scattering particles. The calculation is performed for the spectrum shown in Figure 6 and corresponds to the measurements shown in Figure 12.